NeuroImage 63 (2012) 47–53

Contents lists available at SciVerse ScienceDirect

NeuroImage

journal homepage: www.elsevier.com/locate/ynimg

Deformation-based brain morphometry in rats

Christian Gaser [a,b,*,1], Silvio Schmidt [a,1], Martin Metzler [a], Karl-Heinz Herrmann [c], Ines Krumbein [c], Jürgen R. Reichenbach [c], Otto W. Witte [a]

[a] Hans Berger Clinic for Neurology, Jena University Hospital, Erlanger Allee 101, 07747 Jena, Germany
[b] Department of Psychiatry, Jena University Hospital, Jahnstrasse 3, 07743 Jena, Germany
[c] Medical Physics Group, Department of Diagnostic and Interventional Radiology I, Jena University Hospital, Philosophenweg 3, 07743 Jena, Germany

ARTICLE INFO

Article history:
Accepted 28 June 2012
Available online 6 July 2012

Keywords:
Brain
Magnetic resonance imaging (MRI)
Rat
Deformations-based morphometry (DBM)
Registration

ABSTRACT

Magnetic resonance imaging (MRI)-based morphometry provides in vivo evidence for macro-structural plasticity of the brain. Experiments on small animals using automated morphometric methods usually require expensive measurements with ultra-high field dedicated animal MRI systems. Here, we developed a novel deformation-based morphometry (DBM) tool for automated analyses of rat brain images measured on a 3-Tesla clinical whole body scanner with appropriate coils. A landmark-based transformation of our customized reference brain into the coordinates of the widely used rat brain atlas from Paxinos and Watson (Paxinos Atlas) guarantees the comparability of results to other studies. For cross-sectional data, we warped images onto the reference brain using the low-dimensional nonlinear registration implemented in the MATLAB software package SPM8. For the analysis of longitudinal data sets, we chose high-dimensional registrations of all images of one data set to the first baseline image which facilitate the identification of more subtle structural changes. Because all deformations were finally used to transform the data into the space of the Paxinos Atlas, Jacobian determinants could be used to estimate absolute local volumes of predefined regions-of-interest. Pilot experiments were performed to analyze brain structural changes due to aging or photothrombotically-induced cortical stroke. The results support the utility of DBM based on commonly available clinical whole-body scanners for highly sensitive morphometric studies on rats.

Introduction

Recent magnetic resonance imaging (MRI)-based morphometric studies in humans have shown that changes of the brain's morphology correlate with behavioral abilities, learning, diseases and age (for review see: Fields, 2011; Mietchen and Gaser, 2009; Raz and Rodrigue, 2006). Findings from this field of research have provided new and surprising insights into how the brain reorganizes under native and pathological conditions, and may be highly relevant for the improvement of therapeutic interventions for aging- or disease-induced disabilities. However, the cellular mechanisms underlying macro-structural plasticity in the human brain are largely unknown because their investigation would require *post-mortem* or biopsy tissue samples. To bridge this gap, the transfer of human study designs to animal experiments is urgently required.

Morphometry of animal brain magnetic resonance (MR) images is not straightforward regardless of whether the analysis strategy is region-of-interest (ROI) based or ROI independent. The ROI-based manual outlining of individual brain structures enables the estimation of absolute volumes but requires well-reasoned and time-consuming area demarcation, and the outlining protocols may not be compatible between different laboratories (Foldi et al., 2010; Hasegawa et al., 2010; Henke et al., 2008; Nagel et al., 2004; Sawiak et al., 2009a; Schubert et al., 2008, 2009). Unfortunately, manual approaches fail if the volumes of selected structures differ partially by small amounts. The detection of such diffuse and spatially distributed volume changes over the whole brain requires more sensitive and preferably automated methods. For this purpose, two MR image intensity-based techniques have been developed enabling the quantitative estimation of structural changes. Voxel-based morphometry (VBM) is based on automatic segmentation of the brain in gray matter, white matter and ventricles, and therefore requires high contrast between tissue borders. In small rodents, which are largely preferred for animal experiments on mammals, this is only achievable using ultra-high field MRI systems (preferably >9 T) (Li et al., 2009) or unfeasibly long acquisition times (Sawiak et al., 2009b). In contrast to VBM, deformation-based morphometry (DBM) detects structural differences independent of sharp tissue borders by analysis of deformations needed to match one brain onto a reference brain by nonlinear registration (Ashburner et al., 1998; Gaser et al.,

* Corresponding author at: Department of Psychiatry, Jena University Hospital, Jahnstrasse 3, 07747 Jena, Germany. Fax: +49 3641 934755.
E-mail addresses: christian.gaser@uni-jena.de (C. Gaser), silvio.schmidt@med.uni-jena.de (S. Schmidt), Martin.Metzler@uni-jena.de (M. Metzler), karl-heinz.Herrmann@med.uni-jena.de (K.-H. Herrmann), Ines.Krumbein@med.uni-jena.de (I. Krumbein), Juergen.Reichenbach@med.uni-jena.de (J.R. Reichenbach), Otto.Witte@med.uni-jena.de (O.W. Witte).
[1] Both authors contributed equally.

1053-8119/$ – see front matter © 2012 Elsevier Inc. All rights reserved.
doi:10.1016/j.neuroimage.2012.06.066

1999). Therefore, DBM might be preferable for morphometry of brain structures with lower contrast between different tissues.

The first aim of the present study was to establish a DBM tool for rat brains measured on a 3-Tesla clinical whole body scanner, whereby – by using appropriate coils – we are able to generate images with adequate spatial resolution and tissue contrast in short measurement times (Herrmann et al., 2011). Although DBM was established for mice measured on ultra-high field animal MRI systems (Badea et al., 2010; Carroll et al., 2011; Lau et al., 2008; Lerch et al., 2008; Maheswaran et al., 2009; Mercer et al., 2009; Nieman et al., 2007; Seminowicz et al., 2009; Spring et al., 2010; Verma et al., 2005; Yu et al., 2011; Zhang et al., 2010), the use of clinical scanners for animal studies holds important advantages. First, well-established optimized clinical protocols with sequences that sometimes do not have corresponding counterparts on animal scanners in combination with the lower field strengths with all their benefits on T1 and T2 relaxation times bring the experiments closer to human imaging. Secondly, the large bore size facilitates easier access to the animal and provides more space for equipment necessary for anesthesia supply or animal fixation (Herrmann et al., 2011). Finally, for most researchers, clinical scanners are more easily available than expensive ultra-high field animal MRI systems. The second aim of the study was to implement the advantages of both the ROI-based strategy to estimate absolute volumes and the ROI-independent strategy of qualitative brain morphology to analyze diffuse volume changes which works within the standardized coordinates of the Paxinos Atlas.

For DBM, we adopted a tool that we have previously developed for use with human data (Gaser et al., 2001). A customized rat reference brain was created and landmark-based transformed into the space of the Paxinos Atlas with predefined ROIs. The transformation of deformations into the space of the Paxinos Atlas enables the estimation of absolute local volumes. In a pilot study, we analyzed whole brain and cortical volumes of young adult (3 months) and aged (26 months) male rats in a cross-sectional design and validated the approach by comparing the automatically generated data with results of manual volume estimation. For the detection of more subtle volume changes, we pair-wisely registered longitudinally acquired images of one data set to the first baseline image. The intra-pair deformations are then transformed into the space of the Paxinos Atlas using normalization parameters obtained with the baseline image. We tested this approach on animals with photothrombotically-induced cortical stroke and found a pattern of progressive volume changes in remote non-lesion areas which correlated with recent histologic, physiologic and behavioral findings. To the best of our knowledge, this is the first report demonstrating high sensitivity of DBM in combination with rats measured on a clinical whole body scanner. This novel DBM tool could facilitate the analyses of macro-structural brain plasticity undertaken by other research groups.

Materials and methods

The experiments were performed with male Han–Wist rats in adherence with local government requirements and according to approved guidelines. To compare the macro-structure of young adult and aged brains in a cross-sectional design, MRI was performed on one group of 3-month-old rats (n = 10) and on a second group of 26-month-old rats (n = 15). For longitudinal analysis of stroke-induced brain tissue shrinkage, five consecutive MRI measurements were performed on a group of young adult rats, respectively, one week before (baseline measurement) as well as one, two, four and eight weeks following cortical photothrombotic lesion induction (lesioned: n = 8; controls: n = 8; age at lesion induction: 3 months).

Photothrombotic lesion

Photothrombotic lesions including the primary and secondary motor cortex (M1, M2) as well as parts of the primary somatosensory cortex of the fore- and hindlimbs (S1FL, S1HL) were induced as described previously (Schmidt et al., 2011). In brief, rats were anesthetized with isoflurane (2.5% in oxygen), the skin above the skull was incised and a fiber-optic bundle (aperture: 3.0 mm; light source: Schott KL 1500) was positioned 0.5 mm anterior to bregma and 3.7 mm lateral to midline. During the first minute of illumination (whole illumination time: 20 min), the photosensitive dye rose bengal (Aldrich Chemie, 1.3 mg/100 mg bodyweight) was injected through the tail vein. Body temperature was controlled rectally and held constant at 37 °C. After illumination, the wounds were sutured and animals were placed in a warm environment for approximately 30 min before returning to home cages with free access to food and water. Control animals received the same procedure without injection of the photosensitive dye.

MRI acquisition protocols

Rat brain MRI was performed on a clinical 3 T whole body scanner (Magnetom TIM Trio, Siemens Medical Solutions, Erlangen, Germany) as previously described (Herrmann et al., 2011). For cross-sectional analysis of age-specific brain volume changes, a two-module multi-functional 8-channel surface coil (CPC coil, Noras MRI products GmbH, Höchberg, Germany) was used. Measurements for longitudinal analysis of stroke-induced brain volume changes were performed using a dedicated rat head coil with a linearly polarized Litz coil volume resonator design (Doty Scientific Inc., Columbia, SC, USA). Anesthesia of freely breathing animals was provided by isoflurane (1.7% in oxygen, 1.5 l/min). T2-weighted images were obtained using a 3D SPACE (Sampling Perfection with Application-Optimized Contrasts Using Different Flip Angle Evolutions) sequence (Siemens Healthcare, Erlangen, Germany) with an isotropic resolution of 0.33 mm^3 (matrix $192\times130\times96$, FoV $64\times43\times32$ mm, bandwidth 145 Hz/px, $T_E/T_R = 352$ ms/2500 ms, flip angle mode 'T2var', echo spacing of 10.7 ms, turbo factor of 67 and Partial Fourier of 7/8 in both phase encode directions). While the CPC coil measurements were performed using three repetitions each consisting of two averages with a total acquisition time $T_A = 42$ min, the improved signal-to-noise ratio (SNR) performance of the Doty coil enabled a protocol with two repetitions (one average) with $T_A = 14$ min.

Generation of the reference brain

Because we obtained our T2-weighted images on a clinical 3 T scanner, these images might differ in tissue contrast, spatial resolution and SNR from data acquired on high field scanners. Thus, we could not use any existing rat reference brain and the creation of a customized reference brain was mandatory. We used 176 rats (69 Rcc–Wist, 107 Han–Wist, age range 3–6 months, mean age 3.64 months) to create a customized reference brain. We used two different rat strains to provide a mixed template for future studies that can be used for both Rcc–Wist as well as Han–Wist rats. Another reason to use two strains was to have a large, representative number of rats that are used to create the template. However, the differences between both strains might be rather small because both are substrains from Wistar rats.

The generation of this initial reference brain involved the following steps:

1. Selection of one representative rat brain as reference for initial affine spatial transformation using 12 parameters (Fig. 1A)
2. Manual drawing of a brain mask to exclude non-brain regions from spatial transformation
3. Affine transformation of all brains to the brain from step 1 (Fig. 1A)
4. Calculation of the average of the affine transformed brains to be subsequently used as new reference brain
5. Nonlinear spatial transformation of all brains to the new reference image from step 4
6. Calculation of average of nonlinearly transformed brains to create a new reference brain (Fig. 1B)

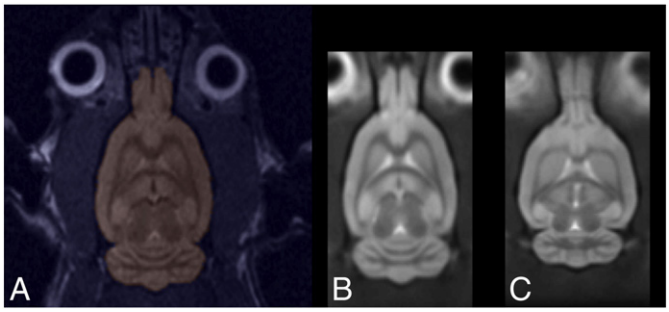

Fig. 1. Creation of reference brain. (A) One representative rat brain was selected as reference for initial affine transformation. A manually drawn brain mask (to exclude non-brain regions from spatial transformation) is overlaid in red colors. (B) The mean image of all nonlinearly transformed images is calculated to create a new reference brain. (C) This image shows the reference brain after transformation into the coordinates of the Paxinos Atlas. (For interpretation of the references to color in this figure legend, the reader is referred to the web version of this article.)

As nonlinear transformation we used the default spatial normalization implemented in the MATLAB software package SPM8 with the following parameters: spatial cut-off 1.5 mm; 24 iterations; regularization of registration 0.1; voxel size for writing $0.2 \times 0.2 \times 0.2$ mm^3; image and template smoothing with FWHM of 0.8 mm; template weighting with the manually defined brain mask. For affine as well as nonlinear transformation a Gauss–Newton optimization was used with least-squares as similarity metric.

This initial reference brain represents the average of 176 brains while providing reasonable spatial details due to the use of a nonlinear spatial transformation. However, the reference space is now primarily defined by the first selected reference brain and is not comparable to other atlases. In order to provide a standardized reference atlas, we made use of the Paxinos Atlas, which is also available as single slice images in JPEG format (Paxinos and Watson, 2005). This atlas is widely used and guarantees standardization and comparability of results. In order to use the Paxinos Atlas, we applied the following procedure:

1. Thresholding and morphological erosion of Paxinos Atlas image slices by one pixel to enlarge borders between regions and provide clear delineation between regions (e.g. regions should be unconnected after erosion)
2. Manual filling of regions slice-by-slice with predefined intensity values for each hemisphere to differentiate between regions (Fig. 2B)
3. Morphological dilation of edited slices by one pixel to refill borders between regions (Fig. 2C)
4. Filling existing gaps between thicker slices with duplicates
5. Combination of all processed slices to a 3D volume with final in-plane resolution of 0.025 mm and a slice thickness of 0.12 mm

Because of the time-consuming and demanding nature of the task, not all regions of the original Paxinos Atlas were used and manually filled. However, all regions in the cortical band were covered, while most of the smaller regions around the midline were not used because of their small size.

In order to transform the initial reference brain into the space of the Paxinos Atlas, we applied a landmark-based thin-plate spline warping (Bookstein, 1989). First, we manually defined 118 corresponding landmarks in both images. Secondly, a thin-plate spline warping was applied to nonlinearly transform the reference brain into the space of the Paxinos Atlas using the Minc-software Register (http://www.bic.mni.mcgill.ca/ServicesSoftware/MINC).

After this final nonlinear registration, the initial reference brain is transformed into the space of the Paxinos Atlas and can now be used as standard reference brain for all rat brains. Finally, the location of the bregma ± 0 in coronal slices was set as origin.

DBM

In order to analyze rat brain structure, we used a DBM approach that we have previously developed for use with human brain data. DBM is a useful technique to detect structural differences over the entire brain since it analyzes positional differences between every voxel and a reference brain. The idea is to use a nonlinear registration to deform one brain onto a reference brain. After this registration, the morphological differences between both brains are minimized and the deformations now encode information about these differences. The Jacobian determinant can be finally used to calculate local volume changes at every voxel. Our DBM approach was validated in an earlier study by comparing the deformation fields and its Jacobian determinant with manually traced ventricular volumes (Gaser et al., 2001).

The accuracy (how detailed will a DBM approach work) mainly depends on the dimensionality of the nonlinear registration that is used to deform the brains. We used two nonlinear registration techniques that differ in terms of dimensionality to provide appropriate approaches for cross-sectional as well as for longitudinal data. For cross-sectional data, we applied the low-dimensional nonlinear registration that is also used in SPM8 as the default registration to spatially normalize data to a reference brain (Ashburner and Friston, 1999). We modified the parameters to work with the deviating dimensions of rat brains with the settings that were described in Generation of the reference brain section: spatial cut-off 1.5 mm; 24 iterations; regularization of registration 0.1; voxel size for writing $0.2 \times 0.2 \times 0.2$ mm^3; image and template smoothing with FWHM of 0.8 mm; template weighting with the manually defined brain mask.

For longitudinal data, more subtle changes are expected. Therefore, we chose a high-dimensional registration with more detailed deformations (Ashburner et al., 1999). This registration allows the identification of more subtle structures with greater precision. A prerequisite for longitudinal data is that all images of one data set are rigidly registered to the first baseline image. After this positional correction, the pair-wise deformations are obtained between all subsequent images of one data set to its baseline. Finally, all intra-pair deformations are nonlinearly transformed to the Paxinos Atlas using the normalization parameters obtained with the baseline image.

Finally, the Jacobian determinant of the deformations can be used to calculate local volume changes. Because all deformations were transformed to the Paxinos Atlas, this atlas can also be used to estimate local volumes of predefined ROIs. That means that for all regions

Fig. 2. Paxinos Atlas. (A) One arbitrary slice from the Paxinos Atlas that is provided as single image for each slice. (B) After thresholding and morphological erosion, borders are enlarged and remaining regions are filled with predefined intensity values. (C) The final Paxinos Atlas is obtained after the borders have been filled with morphological dilation.

defined in our Paxinos Atlas, region-wise volume changes can be estimated and analyzed.

Cavalieri volume estimation

To validate our rat DBM approach, we performed a manual Cavalieri volume estimation on MR images of 10 young adult (3 months) and 15 aged (26 months) rats using the Image J software. By using a 1750 µm size counting frame for the whole brain and a 840 µm size counting frame for the left or right whole cortex, between 948 and 1161 grid points from 27 to 30 coronal sections (block advance: 900 µm) and between 488 and 608 grid points from 16 to 19 coronal sections were counted for the whole brain and the whole cortex, respectively, which provided coefficient of error estimates of <0.1.

Statistical analysis

Voxel-wise analysis of volume changes over time was performed within SPM8 with a repeated measure ANOVA. Only results exceeding a threshold of $p<0.001$ (corrected for multiple comparisons using family-wise error [FWE]) were reported. Results were overlaid onto the average of all normalized anatomical images. We applied a *t*-test to investigate an interaction between time and group by testing for a volume decrease between the first and last time point in the lesion group compared to the control group. Region-wise analysis was obtained using SPSS at a threshold of $p<0.05$.

Results

Cross-sectional analysis

To validate our DBM approach, we determined the volume of young adult and aged rat brains using the cross-sectional design. As shown in Table 1 and Fig. 3, whole brains of 26-month-old rats (3058 ± 22 mm^3, $n=15$) were approximately 12% larger than brains of 3-month-old rats (2741 ± 34 mm^3, $n=10$, $p<0.05$) and showed a slight asymmetry in favor of the right hemisphere ($p<0.05$). The cerebral cortex was chosen as the model structure to illustrate regional analysis. Aged rats showed bi-hemispherically increased cortical volumes of around 6% (~20 mm^3) compared to young adult rats, with the same asymmetry as found for the whole brain ($p<0.05$). Separation into iso- and allocortex (allocortex exclusively constituting the hippocampus), representing phylogenetically new and old parts of the cortex, respectively, revealed that the volume increases as well as the asymmetry resulted mainly from the growth of phylogenetically old allocortical structures. However, cortical volume normalized to the whole brain volume demonstrated that the percent amount of cortical tissue was decreased in aged animals for both iso- and allocortical regions.

To test the reliability of our DBM approach, we compared the automatically determined volumes with results from manual volumetry determined using Cavalieri estimation. Linear regression analysis of both whole brain data ($r=0.98$; $p<0.0001$) and regional data of left and right cortices ($r=0.92$; $p<0.0001$) showed highly significant values (Fig. 4).

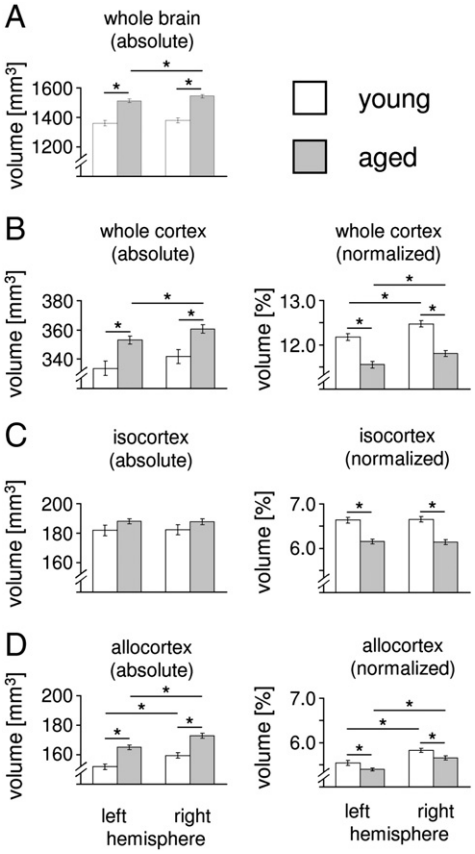

Fig. 3. Age effects. Brain volume of young adult (3 months) and aged (26 months) rats determined by cross-sectional DBM analysis in absolute values and for cortical substructures additionally normalized to the whole brain volume in percent amounts. Aged rats showed larger whole brains (A) and cortices (B) compared to young adults and a slight asymmetry in favor of the right hemisphere. The larger cortices of aged rats did not result from isocortical (C) but mainly from the growth of phylogenetically old allocortical substructures (D). In contrast to absolute volumes, the percent amount of cortical tissue was decreased in aged animals for both iso- and allocortical regions. Significant differences are indicated by asterisks (mean ± SEM, $p<0.05$, unpaired Student's *t*-test).

Longitudinal analysis

The longitudinal tool enables us to analyze more subtle and diffuse volume changes that are not restricted to predefined regions. Here, we screened brains to find areas with tissue shrinkage after right-hemispheric cortical lesioning. The lesion damaged the motor cortex (M1, M2) and parts of the fore- and hindlimb primary somatosensory cortex (S1FL, S1HL). At a threshold of $p<0.001$ (FWE corrected), both hemispheres showed progressive regional tissue shrinkage (Table 2).

Table 1
Volume of selected structures of young adult and aged rat brains.

Brain region	Absolute volume [mm^3]				Normalized volume [%]			
	Young		Aged		Young		Aged	
Whole brain	2741 ± 34		3058 ± 22		100		100	
	Left	Right	Left	Right	Left	Right	Left	Right
Whole hemisphere	1361 ± 18	1380 ± 17	1513 ± 11	1545 ± 12				
Whole cortex	334 ± 5	342 ± 5	353 ± 3	361 ± 3	12.18 ± 0.08	12.47 ± 0.08	11.55 ± 0.08	11.80 ± 0.07
Isocortex	182 ± 4	182 ± 3	188 ± 2	188 ± 2	5.54 ± 0.05	5.82 ± 0.05	5.40 ± 0.04	5.65 ± 0.04
Allocortex	152 ± 2	159 ± 2	165 ± 1	173 ± 2	6.63 ± 0.06	6.65 ± 0.06	6.15 ± 0.05	6.14 ± 0.05

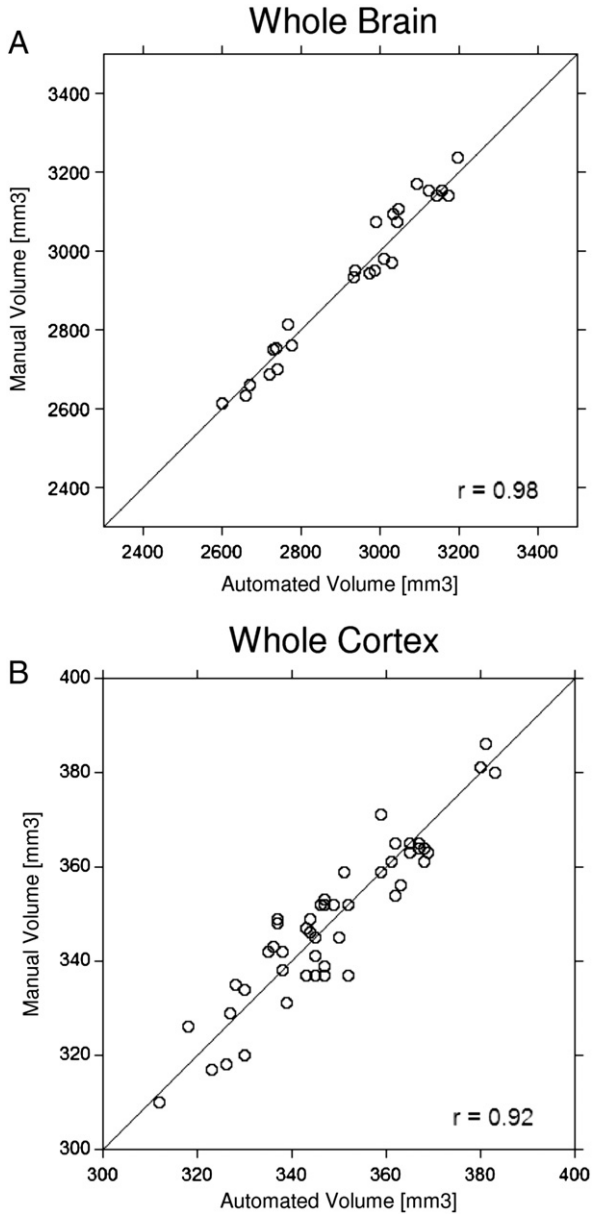

Fig. 4. Validation with Cavalieri method. The correlations between volumes derived from automated cross-sectional DBM analysis and manual Cavalieri volume estimation for whole brain (A) and whole cortex (B) show highly significant values.

Parts of the corpus callosum, the hippocampus, the temporal association cortex, the olfactory tubercle, the insular cortex and anterior parts of the basal ganglia were affected ipsilesionally, whereas more posterior areas of the basal ganglia were affected bilaterally.

Table 2
Areas affected by tissue shrinkage after a cortical infarct in young adult animals.

Brain region	Side	Coordinates			T-Score	Cluster (Voxel)
Corpus callosum	R	3	−1	−4	9.43	48
Hippocampus	R	4	−8	−4	9.12	79
Caudate putamen	R	2	−1	−6	8.43	60
Caudate putamen	L	−6	−3	−6	7.65	56
Caudate putamen	R	5	−3	−5	7.60	65
Temporal association cortex	R	6	−8	−4	7.52	57
Olfactory tubercle	R	3	1	−8	7.50	35
Insular cortex	R	6	−4	−7	7.29	43

Repeated measure ANOVA at a threshold of $p<0.001$ (FWE corrected); *t*-test for volume decrease between the first and last time point in the lesion group compared to the control group.

Fig. 5 illustrates an example of the time-course of volume changes in the ipsilesional hippocampus. Following initial swelling, progressive tissue shrinkage was found in caudal parts of the hippocampus. The volume decreased most strongly between 7 and 14 days following lesion induction and this shrinkage was preserved up to the end of the investigation period on day 56. In contrast, the control animals exhibited a steady volume increase throughout the investigation period, attributed to the continuous growth of the young adult rodent brain.

Discussion

We present here a novel general DBM approach applicable to rat brain MR images acquired from standard clinical 3 T scanners. This tool allows automatic detection of diffuse and spatially distributed subtle volume changes in cross-sectional as well as longitudinal designs. In order to enable standardization and comparability of the results, data are transformed into the Paxinos Atlas reference space (Paxinos and Watson, 2005). This atlas also permits estimations of absolute volumes in ROIs that are defined for this atlas.

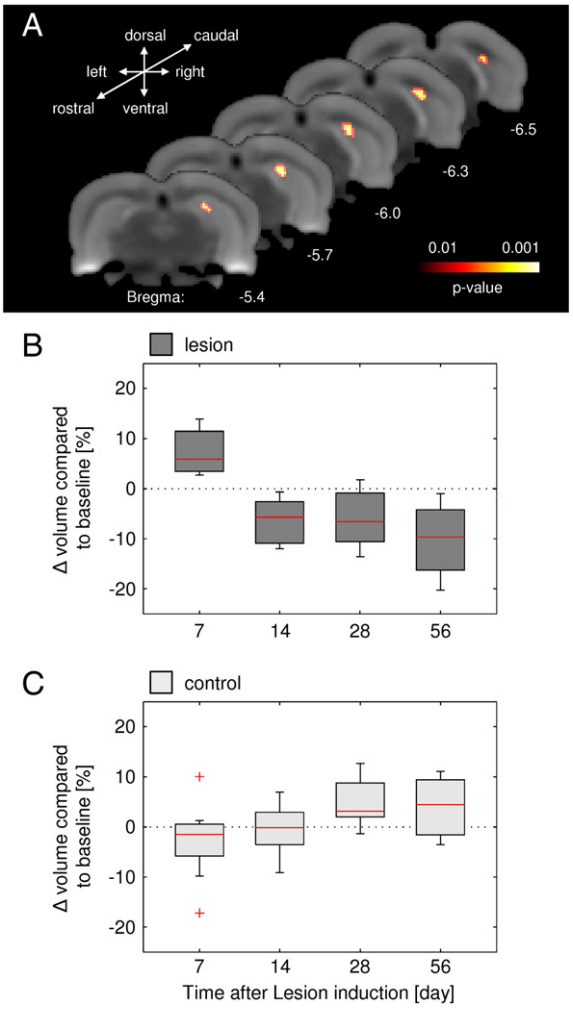

Fig. 5. Time-course of stroke-induced volume changes in the ipsilesional hippocampus. (A) Representative coronal sections between bregma −5.4 and −6.5 showing affected hippocampal areas remote to the cortical lesion that were found to decrease between the first and last time point in the lesion group. The time-courses for the lesion and the control group are illustrated using boxplots, where data between 1.5 and 3 times the interquartile range are indicated by a red "+". The box indicates the 25th and 75th percentile, while the red line relates to the median. (B) In lesioned animals, following initial swelling, we found progressive tissue shrinkage which was preserved up to 56 days. (C) Control animals exhibited increasing volume during the same time period. (For interpretation of the references to color in this figure legend, the reader is referred to the web version of this article.)

To the best of our knowledge, our presented approach is the first that is capable of analyzing rodent data acquired on a standard clinical scanner in an automatic manner. Because dedicated ultra-high field animal MRI systems are expensive and not easily accessible for many research groups, the use of a standard clinical scanner offers many potential applications. One major limitation of the lower field strength, however, is the smaller SNR of the data. Using smaller coils and optimized sequences, the SNR can be increased by up to a factor of 3, which allows acquisition of data with reasonable image quality (Herrmann et al., 2011). Furthermore, the lower SNR can be partially compensated by application of a DBM technique that does not require large image contrasts between tissues compared to VBM methods that rely on segmentation.

The use of a reference atlas is a prerequisite to automatically analyze imaging data. The transformation to an atlas enables standardization and comparability to other studies. We have used the Paxinos Atlas, which is the most common atlas for rats and provides many predefined ROIs. Here, we automated ROI-based morphometry by normalization of brain MR images to the Paxinos reference space that contains the definition of structural borders. By inverting the normalization parameters, prior defined area-borders of the reference space were transferred onto each rat brain. This approach benefits from the resolution of normalization algorithms and therefore exceeds the general accuracy of manual approaches, particularly in areas with lower image contrast. This ROI-based approach has previously been validated by comparing the deformation fields and its Jacobian determinant with manually traced ventricular volumes (Gaser et al., 2001).

In order to validate our approach we have used manual Cavalieri volume estimation and were able to demonstrate a good agreement between these manually derived values and our automatically estimated volumes. However, for future applications registration accuracy might be further increased by the use of advanced template creation approaches that also provide an unbiased average template brain (Kovacevic et al., 2005). For our current template we have used different Wistar rats to provide a mixed template that can be used for both Rcc-Wist and Han–Wist rats. The use of Wistar rats might induce bias in the creation of our template. However, the rats used here are both sub-strains from Wistar rats and the differences between these sub-strains should be rather small. In the future, advanced techniques might help in creating unbiased templates (Ashburner, 2007; Kovacevic et al., 2005) to cover also further strains (Nie et al., in press).

In our cross-sectional study, we found a 12% increase in brain volume in aged rats when compared to younger animals, confirming results of previous MRI-based studies which in a manual (Delatour et al., 2006; Oberg et al., 2008; von Kienlin et al., 2005) or automatic manner (Maheswaran et al., 2009) also determined a linearly increasing volume of the rodent brain during lifespan. In contrast to humans, continuous brain growth in rodents is facilitated by simultaneous expansion of the neurocranium (Sandner et al., 2010). Furthermore, we confirmed results of histological studies that showed rat brain asymmetry (Diamond et al., 1975; Galaburda et al., 1986; Kolb et al., 1982; Rosen et al., 1991, 1993). This anatomic asymmetry is suggested to be an expression of lateralized function (Denenberg, 1983; Rogers, 2006; Sherman and Galaburda, 1984) and can be modulated by practice (Diamond et al., 1987; Dowling et al., 1982). Collectively, the results from our cross-sectional analysis revealed an age-dependent pattern with macro-structural changes of the rat brain, which strongly suggests that ontological features of rodent brain growth should be considered in animal models of age-dependent neurological diseases in humans.

To clarify the causal link between brain structure and behavior, longitudinal measurements are necessary. It has been shown that memorizing for an examination (Draganski et al., 2006) or learning a sensomotory skill is accompanied by temporal transient gray matter expansions in young (Draganski et al., 2004) and aged people (Boyke et al., 2008). These changes peak during the initial 7 days of the learning phase and regress during continued training (Driemeyer et al., 2008). Such a time-course favors rapidly adjusting neuronal systems like spine and synapse turnover as the underlying mechanisms for learning-induced gray matter increases (Trachtenberg et al., 2002). Finally, MRI-based morphometry revealed that both functional plasticity and a structural form of macroscopic brain plasticity are important in processing of information in dynamic networks according to novel informational demands and learning. Longitudinal functional measurements indicate that the functional system involved in recovery may display a great inter-individual variability (Dong et al., 2006; Koski et al., 2004). However, findings based on functional measurements are limited to specific networks activated by the task performed during the experiment. Structural measurements as employed here allow a more global view and might help to predict gains of specific rehabilitation strategies (Lindenberg et al., 2010; Schaechter et al., 2009; Schiemanck et al., 2008; Stinear et al., 2007).

Using our longitudinal approach, we analyzed rat brains for secondary volume changes that were induced by a lesion affecting M1, M2 as well as parts of the S1FL and S1HL cortex. We found a pattern of progressive tissue shrinkage in remote areas that were not primarily affected by the infarct. Most significantly, for gray matter we found time-dependent changes in the ipsilateral hippocampus. Changes initially started with swelling followed by secondary shrinkage of the tissue. It remains unclear which physiological changes are responsible for the volume alterations in the hippocampus and to what extent this influences the improvement of forelimb function after a stroke incident. However, the hippocampal formation appears to be involved in the compensation of impaired functions as well as learning of new strategies to cope with the functional deficit (Chozick, 1983).

The major future challenge is to understand the cellular mechanisms linking macroscopic plasticity measured with MRI in healthy and diseased brains with behavioral consequences. Our approach provides a versatile and valuable tool for research on brain morphology using rats – currently the best animal model for studying the sensory-motor system (Cenci et al., 2002) – in combination with a standard clinical 3 T scanner.

Acknowledgments

This work was supported by BMBF grants 01EV0709, 01GZ0709, 01EO1002 and 0315581B.

We thank Noras MRI products GmbH and Siemens Health Care Sector for their support, and the mechanical workshop of the Friedrich Schiller University Jena for its help in creating various animal head holders.

Appendix A. Supplementary data

Supplementary data to this article can be found online at http://dx.doi.org/10.1016/j.neuroimage.2012.06.066.

References

Ashburner, J., 2007. A fast diffeomorphic image registration algorithm. NeuroImage 38, 95–113.
Ashburner, J., Friston, K.J., 1999. Nonlinear spatial normalization using basis functions. Hum. Brain Mapp. 7, 254–266.
Ashburner, J., Hutton, C., Frackowiak, R., Johnsrude, I., Price, C., Friston, K., 1998. Identifying global anatomical differences: deformation-based morphometry. Hum. Brain Mapp. 6, 348–357.
Ashburner, J., Andersson, J.L., Friston, K.J., 1999. High-dimensional image registration using symmetric priors. NeuroImage 9, 619–628.
Badea, A., Johnson, G.A., Jankowsky, J.L., 2010. Remote sites of structural atrophy predict later amyloid formation in a mouse model of Alzheimer's disease. NeuroImage 50, 416–427.
Bookstein, F.L., 1989. Principal warps: thin-plate splines and the decomposition of deformations. IEEE Trans. Pattern Anal. Mach. Intell. 11, 567–585.
Boyke, J., Driemeyer, J., Gaser, C., Buchel, C., May, A., 2008. Training-induced brain structure changes in the elderly. J. Neurosci. 28, 7031–7035.

Carroll, J.B., Lerch, J.P., Franciosi, S., Spreeuw, A., Bissada, N., Henkelman, R.M., Hayden, M.R., 2011. Natural history of disease in the YAC128 mouse reveals a discrete signature of pathology in Huntington Disease. Neurobiol. Dis. 43 (1), 257–265.
Cenci, M.A., Whishaw, I.Q., Schallert, T., 2002. Animal models of neurological deficits: how relevant is the rat? Nat. Rev. Neurosci. 3, 574–579.
Chozick, B.S., 1983. The behavioral effects of lesions of the hippocampus: a review. Int. J. Neurosci. 22, 63–80.
Delatour, B., Guegan, M., Volk, A., Dhenain, M., 2006. In vivo MRI and histological evaluation of brain atrophy in APP/PS1 transgenic mice. Neurobiol. Aging 27, 835–847.
Denenberg, V.H., 1983. Lateralization of function in rats. Am. J. Physiol. 245, R505–R509.
Diamond, M.C., Johnson, R.E., Ingham, C.A., 1975. Morphological changes in the young, adult and aging rate cerebral cortex, hippocampus, and diencephalon. Behav. Biol. 14, 163–174.
Diamond, M.C., Greer, E.R., York, A., Lewis, D., Barton, T., Lin, J., 1987. Rat cortical morphology following crowded-enriched living conditions. Exp. Neurol. 96, 241–247.
Dong, Y., Dobkin, B.H., Cen, S.Y., Wu, A.D., Winstein, C.J., 2006. Motor cortex activation during treatment may predict therapeutic gains in paretic hand function after stroke. Stroke 37, 1552–1555.
Dowling, G.A., Diamond, M.C., Murphy Jr., G.M., Johnson, R.E., 1982. A morphological study of male rat cerebral cortical asymmetry. Exp. Neurol. 75, 51–67.
Draganski, B., Gaser, C., Busch, V., Schuierer, G., Bogdahn, U., May, A., 2004. Neuroplasticity: changes in grey matter induced by training. Nature 427, 311–312.
Draganski, B., Gaser, C., Kempermann, G., Kuhn, H.G., Winkler, J., Buchel, C., May, A., 2006. Temporal and spatial dynamics of brain structure changes during extensive learning. J. Neurosci. 26, 6314–6317.
Driemeyer, J., Boyke, J., Gaser, C., Buchel, C., May, A., 2008. Changes in gray matter induced by learning—revisited. PLoS One 3, e2669.
Fields, R.D., 2011. Imaging learning: the search for a memory trace. Neuroscientist 17, 185–196.
Foldi, C.J., Eyles, D.W., McGrath, J.J., Burne, T.H., 2010. Advanced paternal age is associated with alterations in discrete behavioural domains and cortical neuroanatomy of C57BL/6J mice. Eur. J. Neurosci. 31, 556–564.
Galaburda, A.M., Aboitiz, F., Rosen, G.D., Sherman, G.F., 1986. Histological asymmetry in the primary visual cortex of the rat: implications for mechanisms of cerebral asymmetry. Cortex 22, 151–160.
Gaser, C., Volz, H.P., Kiebel, S., Riehemann, S., Sauer, H., 1999. Detecting structural changes in whole brain based on nonlinear deformations—application to schizophrenia research. NeuroImage 10, 107–113.
Gaser, C., Nenadic, I., Buchsbaum, B.R., Hazlett, E.A., Buchsbaum, M.S., 2001. Deformation-based morphometry and its relation to conventional volumetry of brain lateral ventricles in MRI. NeuroImage 13, 1140–1145.
Hasegawa, M., Kida, I., Wada, H., 2010. A volumetric analysis of the brain and hippocampus of rats rendered perinatal hypothyroid. Neurosci. Lett. 479, 240–244.
Henke, D., Bottcher, P., Doherr, M.G., Oechtering, G., Flegel, T., 2008. Computer-assisted magnetic resonance imaging brain morphometry in American Staffordshire Terriers with cerebellar cortical degeneration. J. Vet. Intern. Med. 22, 969–975.
Herrmann, K.H., Schmidt, S., Kretz, A., Haenold, R., Krumbein, I., Metzler, M., Gaser, C., Witte, O.W., Reichenbach, J.R., 2011. Possibilities and limitations for high resolution small animal MRI on a clinical whole-body 3T scanner. MAGMA 25 (3), 233–244.
Kolb, B., Sutherland, R.J., Nonneman, A.J., Whishaw, I.Q., 1982. Asymmetry in the cerebral hemispheres of the rat, mouse, rabbit, and cat: the right hemisphere is larger. Exp. Neurol. 78, 348–359.
Koski, L., Mernar, T.J., Dobkin, B.H., 2004. Immediate and long-term changes in corticomotor output in response to rehabilitation: correlation with functional improvements in chronic stroke. Neurorehabil. Neural Repair 18, 230–249.
Kovacevic, N., Henderson, J.T., Chan, E., Lifshitz, N., Bishop, J., Evans, A.C., Henkelman, R.M., Chen, X.J., 2005. A three-dimensional MRI atlas of the mouse brain with estimates of the average and variability. Cereb. Cortex 15, 639–645.
Lau, J.C., Lerch, J.P., Sled, J.G., Henkelman, R.M., Evans, A.C., Bedell, B.J., 2008. Longitudinal neuroanatomical changes determined by deformation-based morphometry in a mouse model of Alzheimer's disease. NeuroImage 42, 19–27.
Lerch, J.P., Carroll, J.B., Dorr, A., Spring, S., Evans, A.C., Hayden, M.R., Sled, J.G., Henkelman, R.M., 2008. Cortical thickness measured from MRI in the YAC128 mouse model of Huntington's disease. NeuroImage 41, 243–251.
Li, Q., Cheung, C., Wei, R., Hui, E.S., Feldon, J., Meyer, U., Chung, S., Chua, S.E., Sham, P.C., Wu, E.X., McAlonan, G.M., 2009. Prenatal immune challenge is an environmental risk factor for brain and behavior change relevant to schizophrenia: evidence from MRI in a mouse model. PLoS One 4, e6354.
Lindenberg, R., Renga, V., Zhu, L.L., Betzler, F., Alsop, D., Schlaug, G., 2010. Structural integrity of corticospinal motor fibers predicts motor impairment in chronic stroke. Neurology 74, 280–287.
Maheswaran, S., Barjat, H., Rueckert, D., Bate, S.T., Howlett, D.R., Tilling, L., Smart, S.C., Pohlmann, A., Richardson, J.C., Hartkens, T., et al., 2009. Longitudinal regional brain volume changes quantified in normal aging and Alzheimer's APP x PS1 mice using MRI. Brain Res. 1270, 19–32.
Mercer, R.E., Kwolek, E.M., Bischof, J.M., van Eede, M., Henkelman, R.M., Wevrick, R., 2009. Regionally reduced brain volume, altered serotonin neurochemistry, and abnormal behavior in mice null for the circadian rhythm output gene Magel2. Am. J. Med. Genet. B Neuropsychiatr. Genet. 150B, 1085–1099.
Mietchen, D., Gaser, C., 2009. Computational morphometry for detecting changes in brain structure due to development, aging, learning, disease and evolution. Front Neuroinformatics 3, 25.
Nagel, S., Wagner, S., Koziol, J., Kluge, B., Heiland, S., 2004. Volumetric evaluation of the ischemic lesion size with serial MRI in a transient MCAO model of the rat: comparison of DWI and T1WI. Brain Res. Brain Res. Protoc. 12, 172–179.
Nie, B., Chen, K., Zhao, S., Liu, J., Gu, X., Yao, Q., Hui, J., Zhang, Z., Teng, G., Zhao, C., Shan, B., in press. A rat brain MRI template with digital stereotaxic atlas of fine anatomical delineations in paxinos space and its automated application in voxel-wise analysis. Hum. Brain Mapp. doi:10.1002/hbm.21511
Nieman, B.J., Lerch, J.P., Bock, N.A., Chen, X.J., Sled, J.G., Henkelman, R.M., 2007. Mouse behavioral mutants have neuroimaging abnormalities. Hum. Brain Mapp. 28, 567–575.
Oberg, J., Spenger, C., Wang, F.H., Andersson, A., Westman, E., Skoglund, P., Sunnemark, D., Norinder, U., Klason, T., Wahlund, L.O., Lindberg, M., 2008. Age related changes in brain metabolites observed by 1H MRS in APP/PS1 mice. Neurobiol. Aging 29, 1423–1433.
Paxinos, G., Watson, C., 2005. The Rat Brain in Stereotaxic Coordinates, 5th edn. Academic Press, San Diego.
Raz, N., Rodrigue, K.M., 2006. Differential aging of the brain: patterns, cognitive correlates and modifiers. Neurosci. Biobehav. Rev. 30, 730–748.
Rogers, L.J., 2006. Factors influencing development of lateralization. Cortex 42, 107–109.
Rosen, G.D., Sherman, G.F., Galaburda, A.M., 1991. Ontogenesis of neocortical asymmetry: a [3H]thymidine study. Neuroscience 41, 779–790.
Rosen, G.D., Sherman, G.F., Galaburda, A.M., 1993. Neuronal subtypes and anatomic asymmetry: changes in neuronal number and cell-packing density. Neuroscience 56, 833–839.
Sandner, G., Angst, M.J., Guiberteau, T., Guignard, B., Brasse, D., 2010. MRI and X-ray scanning images of the brain of 3-, 6- and 9-month-old rats with bilateral neonatal ventral hippocampus lesions. NeuroImage 53, 44–50.
Sawiak, S.J., Wood, N.I., Williams, G.B., Morton, A.J., Carpenter, T.A., 2009a. Use of magnetic resonance imaging for anatomical phenotyping of the R6/2 mouse model of Huntington's disease. Neurobiol. Dis. 33, 12–19.
Sawiak, S.J., Wood, N.I., Williams, G.B., Morton, A.J., Carpenter, T.A., 2009b. Voxel-based morphometry in the R6/2 transgenic mouse reveals differences between genotypes not seen with manual 2D morphometry. Neurobiol. Dis. 33, 20–27.
Schaechter, J.D., Fricker, Z.P., Perdue, K.L., Helmer, K.G., Vangel, M.G., Greve, D.N., Makris, N., 2009. Microstructural status of ipsilesional and contralesional corticospinal tract correlates with motor skill in chronic stroke patients. Hum. Brain Mapp. 30, 3461–3474.
Schiemanck, S.K., Kwakkel, G., Post, M.W., Kappelle, L.J., Prevo, A.J., 2008. Impact of internal capsule lesions on outcome of motor hand function at one year post-stroke. J. Rehabil. Med. 40, 96–101.
Schmidt, S., Bruehl, C., Frahm, C., Redecker, C., Witte, O.W., 2011. Age dependence of excitatory-inhibitory balance following stroke. Neurobiol. Aging 33 (7), 1356–1363.
Schubert, M.I., Kalisch, R., Sotiropoulos, I., Catania, C., Sousa, N., Almeida, O.F., Auer, D.P., 2008. Effects of altered corticosteroid milieu on rat hippocampal neurochemistry and structure—an in vivo magnetic resonance spectroscopy and imaging study. J. Psychiatr. Res. 42, 902–912.
Schubert, M.I., Porkess, M.V., Dashdorj, N., Fone, K.C., Auer, D.P., 2009. Effects of social isolation rearing on the limbic brain: a combined behavioral and magnetic resonance imaging volumetry study in rats. Neuroscience 159, 21–30.
Seminowicz, D.A., Laferriere, A.L., Millecamps, M., Yu, J.S., Coderre, T.J., Bushnell, M.C., 2009. MRI structural brain changes associated with sensory and emotional function in a rat model of long-term neuropathic pain. NeuroImage 47, 1007–1014.
Sherman, G.F., Galaburda, A.M., 1984. Neocortical asymmetry and open-field behavior in the rat. Exp. Neurol. 86, 473–482.
Spring, S., Lerch, J.P., Wetzel, M.K., Evans, A.C., Henkelman, R.M., 2010. Cerebral asymmetries in 12-week-old C57Bl/6J mice measured by magnetic resonance imaging. NeuroImage 50, 409–415.
Stinear, C.M., Barber, P.A., Smale, P.R., Coxon, J.P., Fleming, M.K., Byblow, W.D., 2007. Functional potential in chronic stroke patients depends on corticospinal tract integrity. Brain 130, 170–180.
Trachtenberg, J.T., Chen, B.E., Knott, G.W., Feng, G., Sanes, J.R., Welker, E., Svoboda, K., 2002. Long-term in vivo imaging of experience-dependent synaptic plasticity in adult cortex. Nature 420, 788–794.
Verma, R., Mori, S., Shen, D., Yarowsky, P., Zhang, J., Davatzikos, C., 2005. Spatiotemporal maturation patterns of murine brain quantified by diffusion tensor MRI and deformation-based morphometry. Proc. Natl. Acad. Sci. U. S. A. 102, 6978–6983.
von Kienlin, M., Kunnecke, B., Metzger, F., Steiner, G., Richards, J.G., Ozmen, L., Jacobsen, H., Loetscher, H., 2005. Altered metabolic profile in the frontal cortex of PS2APP transgenic mice, monitored throughout their life span. Neurobiol. Dis. 18, 32–39.
Yu, X., Nieman, B.J., Sudarov, A., Szulc, K.U., Abdollahian, D.J., Bhatia, N., Lalwani, A.K., Joyner, A.L., Turnbull, D.H., 2011. Morphological and functional midbrain phenotypes in Fibroblast Growth Factor 17 mutant mice detected by Mn-enhanced MRI. NeuroImage 56 (3), 1251–1258.
Zhang, J., Peng, Q., Li, Q., Jahanshad, N., Hou, Z., Jiang, M., Masuda, N., Langbehn, D.R., Miller, M.I., Mori, S., et al., 2010. Longitudinal characterization of brain atrophy of a Huntington's disease mouse model by automated morphological analyses of magnetic resonance images. NeuroImage 49, 2340–2351.